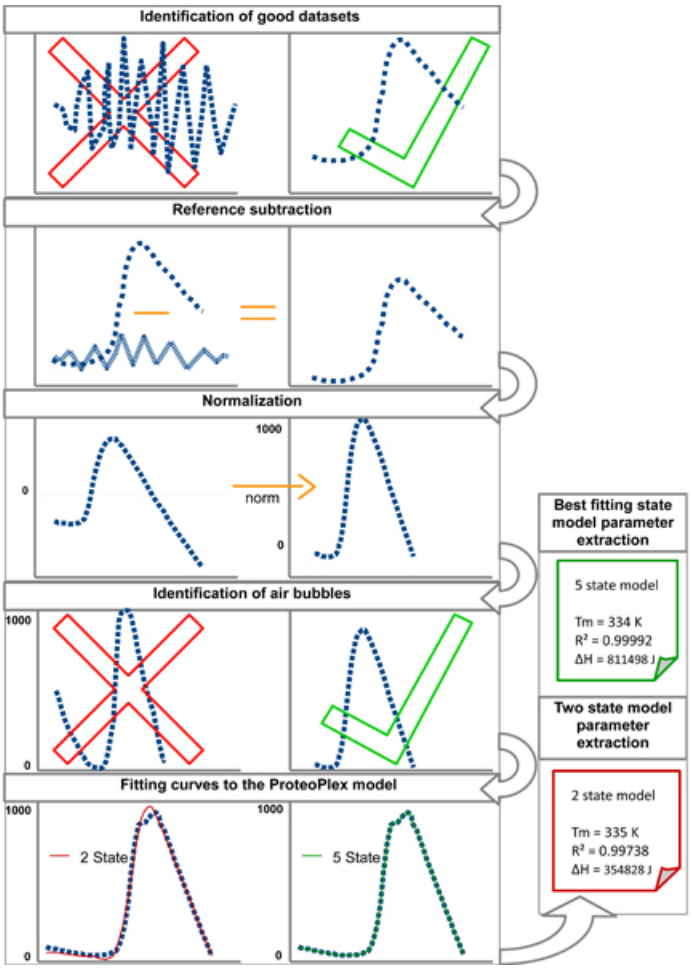

Supplementary Figure 1

Data analysis workflow.

First step: Identification of valid datasets. Amplitudes and number of valid maxima are investigated. If more than 6 local maxima are identified the curve is neglected. **Second step:** Background subtraction. The signal from both buffer references are averaged and subtracted from all individual curves in the dataset. **Third step:** Normalization. All datasets are normalized to a range of 0 to 1000, by setting the lowest local minimum to 0 and the highest relevant local maximum to 1000. **Fourth step:** Identification and removal of datasets containing air bubbles. The slope from the first data-point to the first relevant local minimum is evaluated. Curves with large slopes are omitted. This also removes transitions of proteins, which were already aggregated in solution prior to measurement. **Fifth step:** Data approximation according to the thermodynamic framework presented here for two- to five-state models. **Sixth step:** Parameter extraction for two-state and best fitting models. The values for T_m, ΔH_m, R^2 are extracted for the two-state model and the best fitting model. These extracted parameters are then hierarchically sorted to evaluate the most stabilizing conditions.

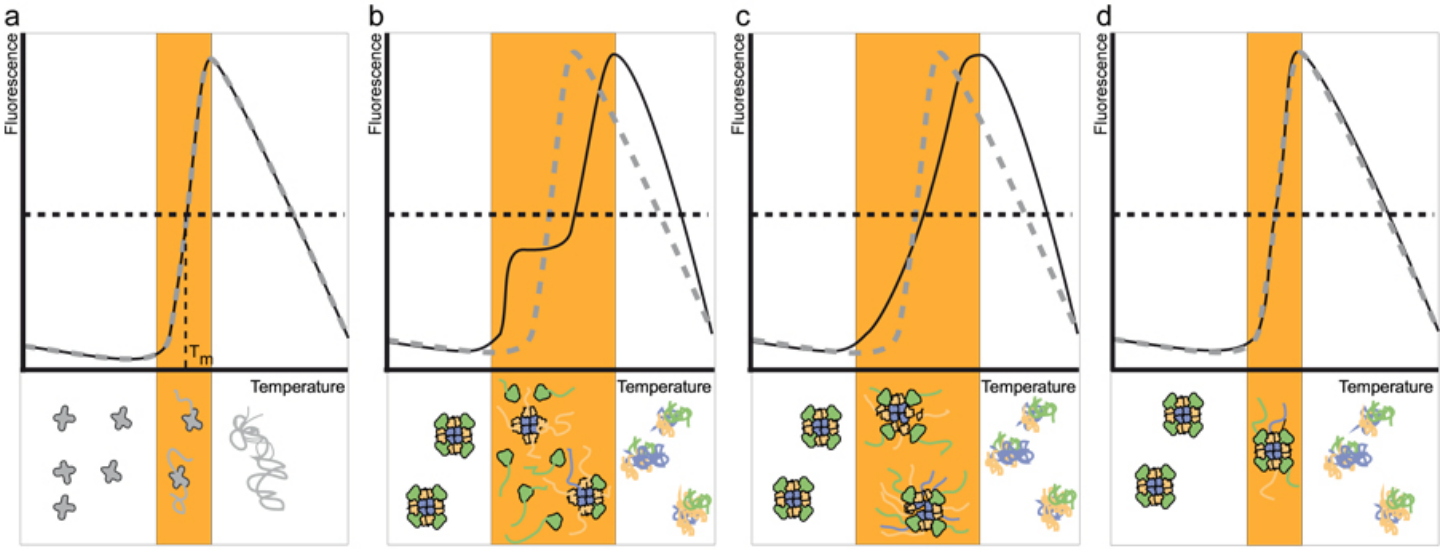

Supplementary Figure 2

Schematic representation of possible unfolding scenarios.

Schematic temperature vs. fluorescence curves are shown, with different colors representing three phases of the entire unfolding transition. The left white part represents the folded phase, the middle orange part the unfolding phase and the right white part the aggregation phase. The half-maximal intensity corresponding to the inflection point of the curve and thus the melting temperature is depicted as dotted line. The dashed line curve insets represent an idealized two state unfolding behavior, with a steep transition. Cartoons of the behavior of proteins are depicted below the graph. (a) A typical unfolding transition curve of a single domain protein is shown. Note, that it overlays well with the dashed line and therefore it is assumed to represent two-state unfolding. (b) The unfolding curve for an instable protein complex is shown. The complex disassembles before it unfolds, yielding multiple transitions and a considerable divergence from two-state unfolding. (c) The unfolding transition for another instable protein complex is shown. Disassembly and unfolding occur in a narrow temperature range yielding multiple transitions which superimpose in a way that they cannot be distinguished anymore. However, this yields a shallow transition in comparison to the dashed line curve (i.e. two-state unfolding). (d) The unfolding curve of a stable complex is shown. Disassembly and unfolding occur in a near concerted manner. Thus, the curve resembles the two-state transition shown in (a).

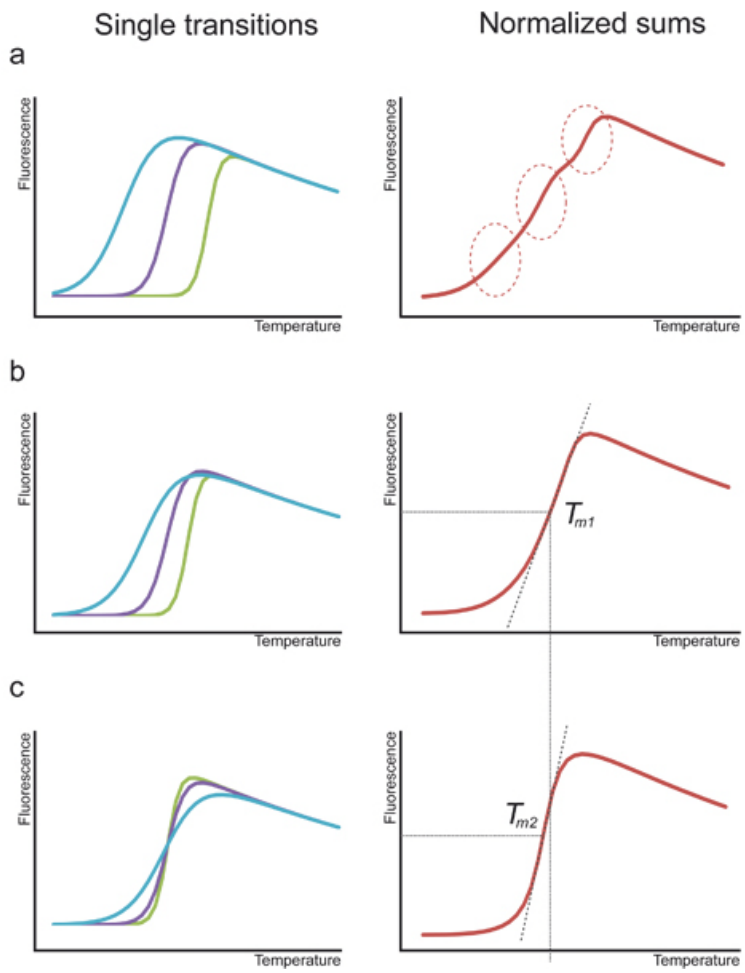

Supplementary Figure 3

Theoretical unfolding transition behaviors.

Temperature – fluorescence unfolding curves of a theoretical three-subunit complex are shown. Left: The single-transitions of the individual components are depicted. Right: Graphs depict a normalized sum of three individual curves. (a) The three components unfold independently from each other at different temperatures. The sum is a curve showing several independent transitions. (b) The components unfold at similar temperatures but still independently from each other. The resulting sum resembles a two-state unfolding curve. (c) The components unfold cooperatively at the same temperature. This also results in a two-state curve, which is steeper than in the middle case. However, the melting temperature of the shallower uncooperative unfolding transitions results in an apparently higher melting point T_{m1}, than the cooperative transition (T_{m2}) as visualized by the dotted lines.

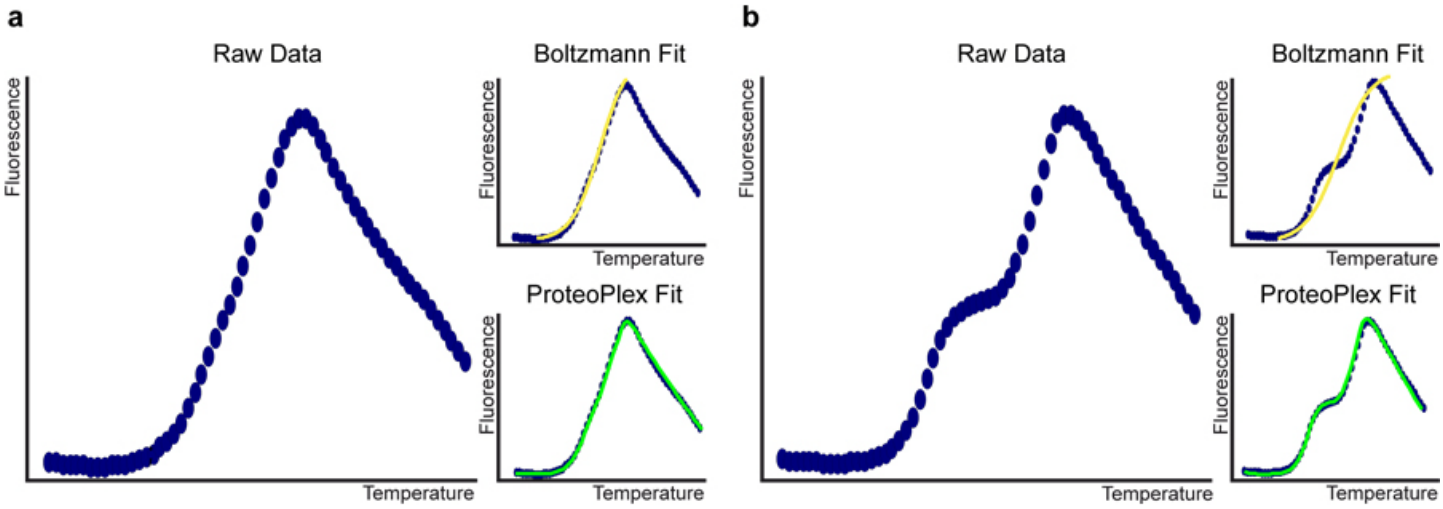

Supplementary Figure 4

Evaluation of the quality of ProteoPlex data approximation.

Two experimental data curves exemplifying the curve fitting process are shown as blue dots. In DSF only the transition part of the data is fitted by a Boltzmann model as shown in yellow[13]. The best data approximation from ProteoPlex is shown in green. While Boltzmann data approximation still gives acceptable results for a near two-state unfolding behavior (left), multiple transitions cannot be approximated by a simple Boltzmann model (right). In contrast, ProteoPlex still describes the obtained curve well. Of note: The ProteoPlex model is able to fit the whole curve and thus will obtain more accurate parameters.

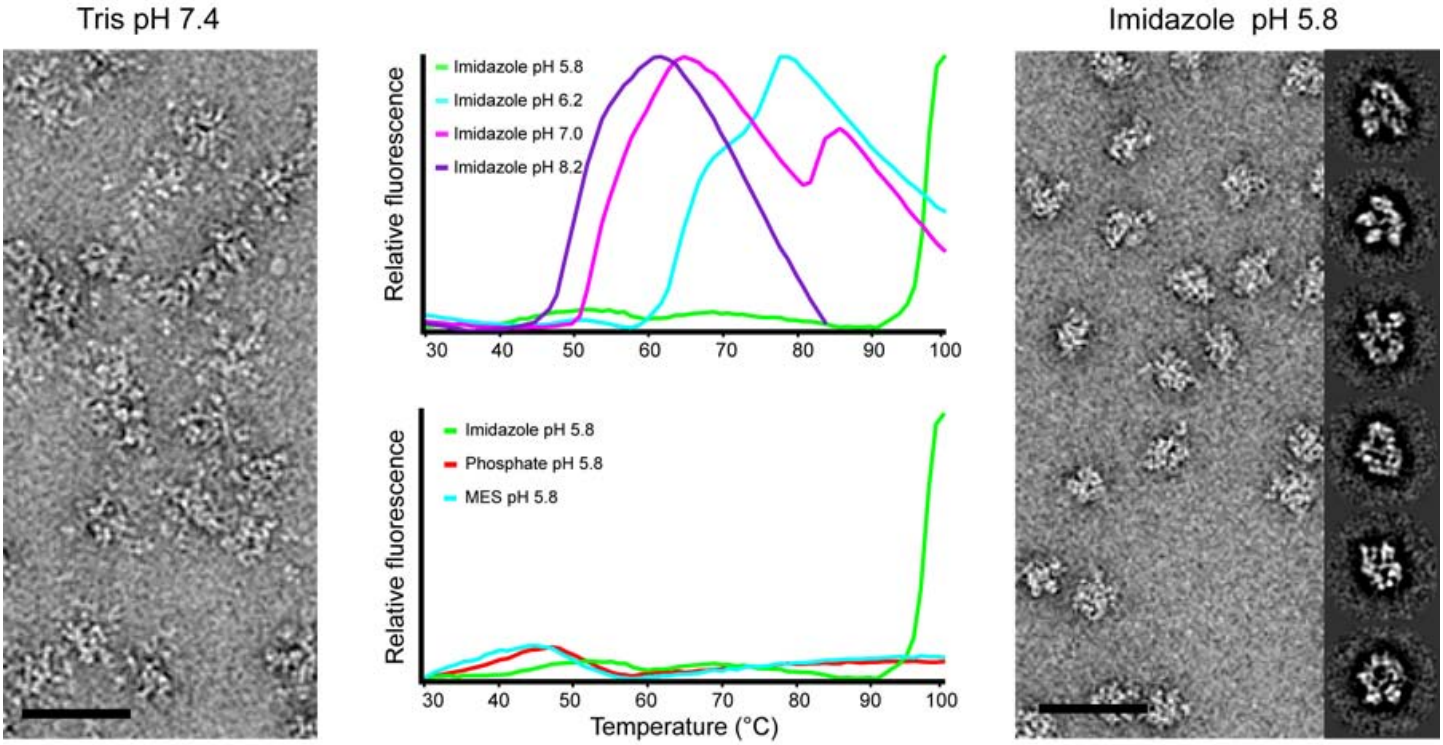

Supplementary Figure 5

Screening for additives.

Analysis of *Biomphalaria glabrata* hemoglobin complex (BgHb, 1.5 MDa native molecular weight) – a protein of unknown structure. Under standard purification conditions BgHb is mostly present as aggregated particles in negatively stained EM images (left panel, scale bar = 50 nm). The upper pane of the middle panel depicts a subset of unfolding transitions from a ProteoPlex pH screen. The stability of BgHb is gradually increased from alkaline to acidic Imidazole buffer conditions, with a final enhanced stabilization of 45 K at pH 5.8 compared to pH 8.2. The lower pane of the middle panel reveals that interpretable unfolding transitions of the complex only occurs in Imidazole buffer, which suggests the role of Imidazole additionally as a stabilizing ligand. In Imidazole pH 5.8, negatively stained EM analysis reveals a monodisperse field of compact particles (right panel, scale bar 50 nm).

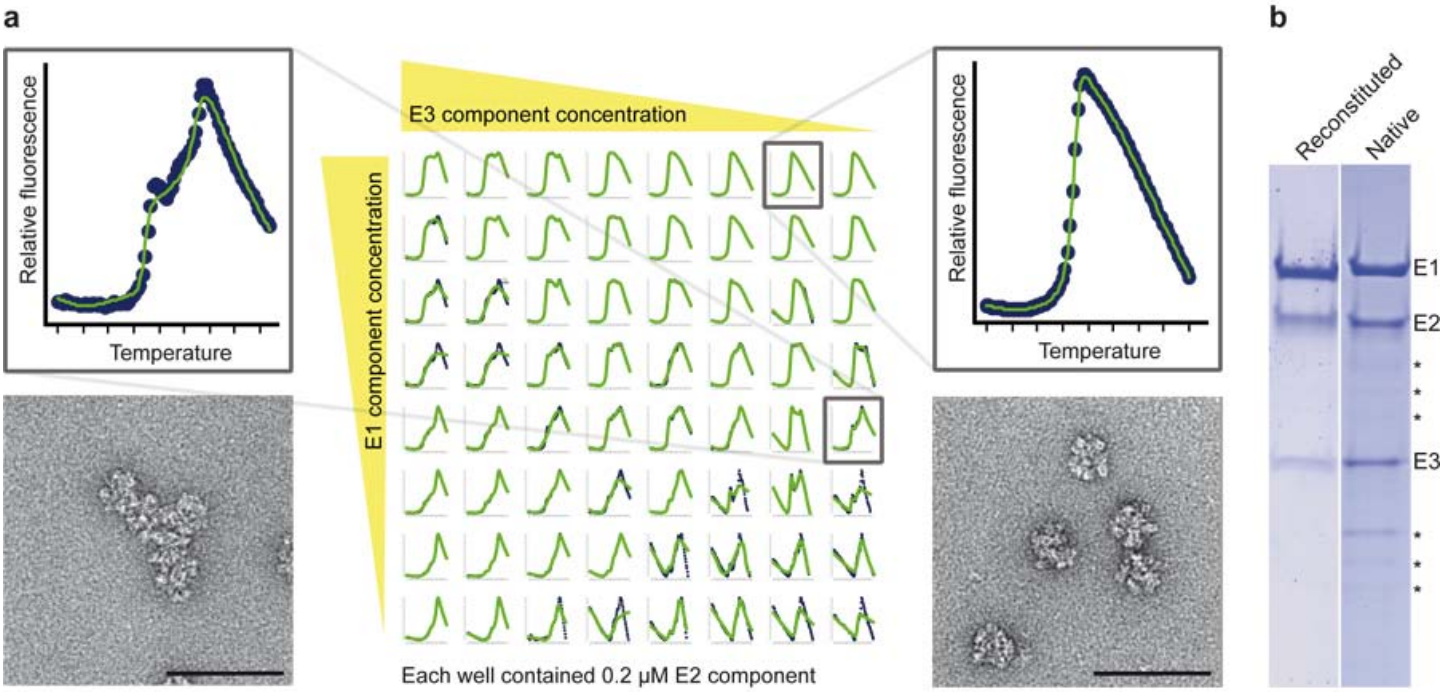

Supplementary Figure 6

Finding optimal conditions for reconstitution experiments.

(a) Reconstitution of PDHc from individually purified subunits (E1, E2, E3). A constant concentration of the core E2 component was mixed with increasing amounts of E1 along the y-axis and increasing E3 amounts along the x-axis (5, 4 and 2.5, 1.5, 1, 0.5, 0.25 and 0.125 fold molar excess of E2 subunit) and assayed with ProteoPlex. Experimental curves (blue dots) and fits (green) from the screen (middle) show two-state unfolding behavior in the case of a high excess of E1 over E2 and low amounts of E3 and mono-disperse, compact particles in EM images (right panel). Whereas, low amounts of E1 and E3 in comparison to E2 yields polyphasic transitions and aggregated particles (left panel).The scalebar corresponds to 50 nm in the EM images. (b) SDS-PAGE of the peak fractions of the reconstituted sample and a sample purified from native source are shown. Asterisks denote impurities in the sample purified from native source. Note the stoichiometry of both samples agree well with each other.

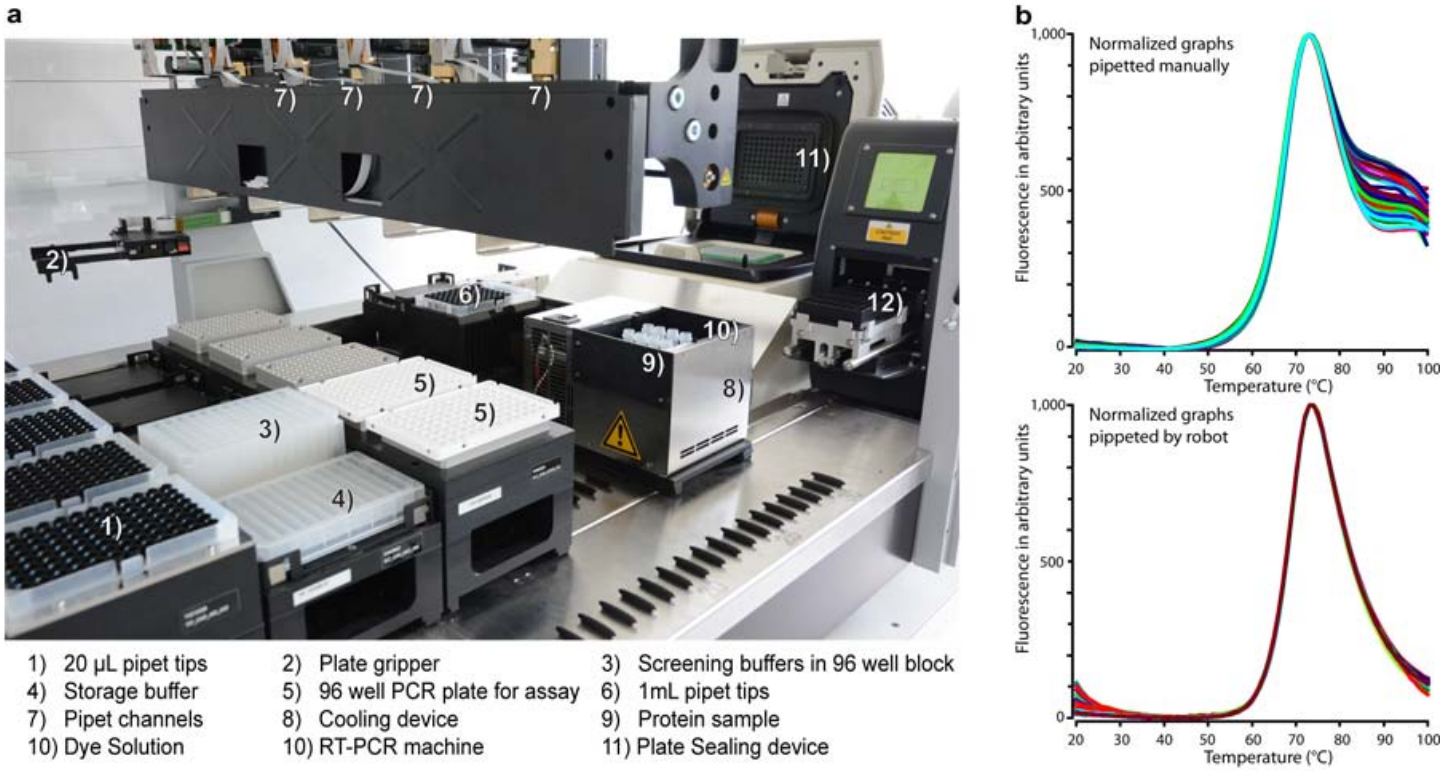

Supplementary Figure 7

Automation.

(a) The robotic platform consists of a liquid handling system a plate sealing device and a RT-PCR machine. The setup allows full automation of liquid handling, thermal melt measurement and data evaluation. **(b)** Reproducibility tests using manual (top panel) and robotic pipetting (lower panel) of 96 identical conditions. The robotic liquid handling reveals a significant increase in reproducibility as shown by an almost perfect overlay of the normalized curves.

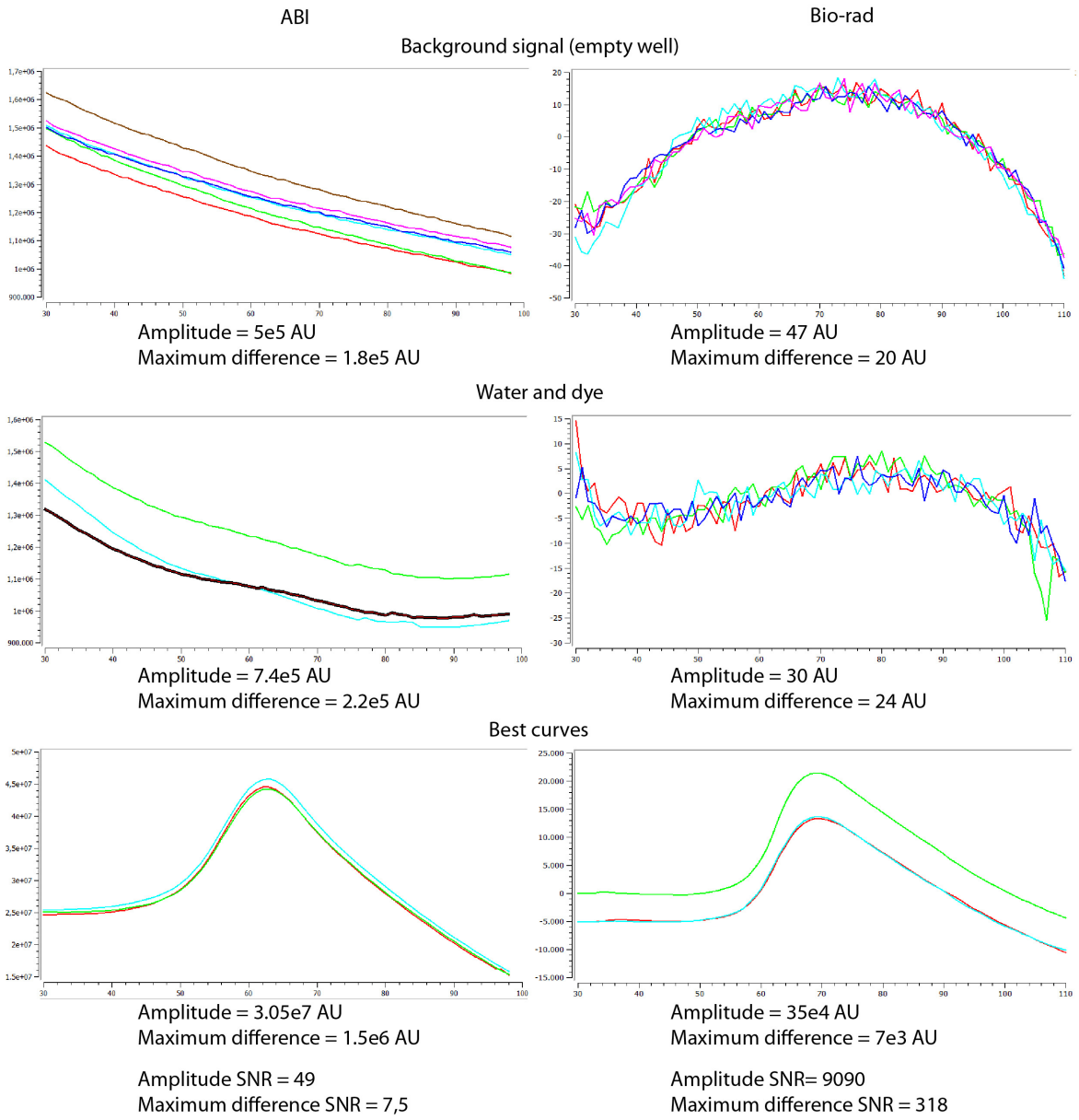

Supplementary Figure 8

Test of different real-time PCR (RT-PCR) machines.

Two of the most commonly used RT-PCR machines were tested towards their applicability with ProteoPlex: the ABI Via7 and the Bio-Rad CFX connect. First the background signal was analyzed. While it was uniform for the Bio-Rad machine (upper row, right panel), strong discrepancies could be seen for the ABI device. A very similar result can be seen by just measuring Sypro Orange diluted to the concentration used for screening (second row). Lastly the machines were tested with Lysozyme and the amplitude of the noise as well of the protein in optimal concentration was measured. A simple SNR was estimated by dividing these two amplitudes. The Bio-Rad machine reaches a SNR that is twice higher than the Via7.

Supplementary Note

A thermodynamic framework to describe unfolding transitions

Present data analysis schemes for the obtained unfolding transitions employ a non-linear regression of curves to a simple Boltzmann model to determine the inflection point during fluorescence increase. This determines the melting point of the protein and has been used as a readout for the stabilization of single-domain proteins[1]. In the main manuscript (Figs. 1c, 2 and Supplementary Fig.6), we have been able to show that when macromolecular complexes are subjected to thermal unfolding in the presence of a solvatochromatic dye, a destabilizing environment is indicated when their subunits unfold in a non-cooperative manner (Fig.1c , 2 and Supplementary Fig.6). Such non-cooperativity in unfolding would yield distinctly polyphasic unfolding transitions for the entire complex, which cannot be properly interpreted by standard DSF analysis because a single inflection point does not exist (Supplementary Fig.3a, normalized sums). The subunits of a macromolecular complex can also either unfold in a non-cooperative manner in a small temperature range (Supplementary Figs. 2b and 3a), a nearly-cooperative (Supplementary Figs. 2c and 3b), or entirely cooperative manner (Supplementary Figs. 2d and 3c). Interpretation of melting curves is challenging, because an apparent two-state unfolding curve can be obtained even for non-cooperative unfolding (Supplementary Fig.3b and c, normalized sums). Note that under stabilizing (near cooperative unfolding) conditions, the apparent melting point can be lower than under uncooperative unfolding conditions (Fig.2a), illustrating that the DSF concept of using the melting point readout for the stabilization of macromolecular complexes is not valid (Supplementary Fig.3, compare normalized sums of b and c). As a consequence, the development of a thermodynamic framework, which is able to approximate experimental data from unfolding transitions of macromolecular complexes, is able to deal with multiple unfolding states and determines those resembling two-state unfolding transitions, is described in the following.

For a classical DSF experiment of a single domain protein the following parameters describe the observed changes in the fluorescent signal. In total, three different species of the solvatochromatic dye can be found at any time point in solution in the course of the experiment: (I) free dye with a maximal fluorescence of F_0, (II) dye bound to the native state of the protein with a maximal signal of F_N, and (III) dye bound to the unfolded protein corresponding to F_U. At each time point, the measured total fluorescence signal can be described by the sum of the signal proportions emitted by

those three species:

$$F = f_N F_N + f_U F_U + F_0 \quad (1)$$

,where f_N and f_U are the fractions of the native and the unfolded protein states, respectively. F_0 does not change during the course of the experiment and can be simply subtracted from the measured data by performing a control experiment in the absence of protein. This behavior is explained by the choice of experimental settings, where the dye is present in a large molar excess of the protein. Forthwith, F_0 can be ignored from further consideration.

Assuming a simple two-state model described by the equilibrium constant $K = f_U/f_N$ equation (1) can be reformulated as follows:

$$F = \frac{F_N + F_U K}{1+K} \quad (2)$$

The experimental settings dictate a strong temperature dependence, which also applies to all equation parameters. Therefore, substitution of the equilibrium constant K in equation (2) using van't Hoff's equation leads to:

$$F = \frac{F_N(T) + F_U(T) e^{-\frac{\Delta G_{U-N}}{RT}}}{1+e^{-\frac{\Delta G_{U-N}}{RT}}} \quad (3)$$

Furthermore, by applying the assumption that the unfolding entropy is temperature independent within the range of measurement, equation (3) can be reformulated as a slight variation of the two-state equation of protein folding [2]:

$$F(T) = \frac{F_N(T) + F_U(T)\, e^{-\frac{\Delta H_m}{RT}\frac{(T-T_m)}{T_m}}}{1+e^{-\frac{\Delta H_m}{RT}\frac{(T-T_m)}{T_m}}} \quad (4)$$

In equation (4), ΔH_m describes the unfolding enthalpy and T_m the melting temperature at which the fraction of native and unfolded protein species are equal. $F_N(T)$ describes the fluorescence at the starting point of the measurement and can be approximated to be linear for most cases. Deviation from this linear behavior can result from solvent exposed hydrophobic molecules like detergents or peptides present in the sample, air bubbles, aggregates in solution, as well as exposed hydrophobic patches in the native state of a protein. A different approximation is required to account for $F_N(T)$ in each of

these cases. Detergent, air bubbles or aggregates result in pronounced light scattering. Correction for these phenomena would introduce a number of unknown parameters into the model, which has led us to omit transitions showing those effects from analysis. $F_U(T)$ describes the aggregation behavior, the rate of which gradually increases. This increase is caused by the incremental rise in temperature during the course of the experiment. Aggregation thus corresponds to the region of the curve, where fluorescence declines. The constant change in the aggregation rate makes it impossible to accurately describe this part of the curve with the available data. Therefore, we approximate the course of the aggregation as a single exponential.
The incorporation of all these correction schemes into equation (4) yields:

$$F(T) = \frac{m_N T + n_N + F_U e^{-rT}\, e^{-\frac{\Delta H_m}{RT}\frac{(T-T_m)}{T_m}}}{1+e^{-\frac{\Delta H_m}{RT}\frac{(T-T_m)}{T_m}}} \qquad (5)$$

Following parameters can be derived from equation (5): The melting temperature of the protein, T_m, which provides a measure for the unfolding entropy, as well as ΔH_m, the unfolding enthalpy. A high T_m and a high ΔH_m are highly indicative of stabilizing conditions. To accurately describe protein stability, one needs to extrapolate the free unfolding enthalpy ΔG_{U-N} to the temperatures desired for structural analysis. If the change in heat capacity during the unfolding process ΔC_p is known, this can be done according to[3]:

$$\Delta G_{U-N}(T) = \Delta H_m \frac{T_m - T}{T_m} - \Delta C_p \left[T_m - T + T \cdot ln\left(\frac{T}{T_m}\right)\right]. \qquad (6)$$

In contrast to the above description, which describes unfolding transitions of single-domain proteins, additional dye states have to be assumed in the case of macromolecular complexes. In principle at any given moment of the measurement, dye molecules can be bound by each individual subunit and each possible permutation of interaction between subunits in both folded and unfolded states. Therefore, equation (1) must be reiterated to:

$$F = \sum_{i=1}^{n} (f_{N,i} F_{N,i} + f_{U,i} F_{U,i}) + F_0, \qquad (7)$$

where *n* is the number of possible transitions. Three different unfolding mechanisms for complexes can be now assumed. (A) The complex disassembles very rapidly due

to the temperature increase, and the components unfold independently. This would lead to a sum of individual unfolding curves and presumably multiphasic transitions (Supplementary Fig.2a). (B) The complex disassembles with a slow rate constant, with some dissociated components already unfolding (Supplementary Fig.2b). As described above, the transitions in this scenario would resemble apparently two-state unfolding behavior without actually being so. (C) Disassembly of the entire complex and unfolding of the complex components occur in a near cooperative manner and therefore concertedly (Supplementary Fig.2c). This would yield two-state unfolding transitions and simultaneously be indicative of stabilizing conditions for the macromolecular complex.

Assuming that no cooperativity exists, the individual components will unfold independently of each other, for which equation (3) can be reformulated as:

$$F(T) = \sum_{i=0}^{n} \frac{F_{N,i}(T)+F_{U,i}(T)\, e^{-\frac{\Delta H_{m,i}}{RT}\frac{(T-T_{m,i})}{T_{m,i}}}}{1+e^{-\frac{\Delta H_{m,i}}{RT}\frac{(T-T_{m,i})}{T_{m,i}}}}. \quad (8)$$

Where $\Delta H_{m,i}$ describes the sum of unfolding and the dissociation enthalpy for each individual component.

In general, one should be able to describe every curve by the ratio of the disassembly equilibria of the entire complex over the unfolding of each individual component given by:

$$F(T) = \sum_{i=1}^{n} \frac{F_{N,i}(T)+F_{U,i}(T)\, e^{-\frac{\Delta H_{m,i}}{RT}\frac{(T-T_{m,i})}{T_{m,i}}}}{1+e^{-\frac{\Delta H_{m,i}}{RT}\frac{(T-T_{m,i})}{T_{m,i}}}} \frac{K_{dis,i}(T)}{1+K_{dis,i}(T)} \text{ with } K_{dis,i}(T) = e^{-\frac{\Delta H_{dis,i}(T-T_{m,dis,i})}{RTT_{m,dis,i}}} \quad (9)$$

In the extreme case, n = 1 equations (8) and (9) become analogous to equation (4). This implies that the unfolding and disassembly of the complex can occur in a cooperative manner. Therefore, under ideal circumstances, it can be assumed that the disassembly of a complex and the unfolding of its components occur concertedly. Equation (4) then provides a suitable description of this phenomenon; with the difference that ΔH_m now describes the weighted mean of all unfolding and dissociation

enthalpies. Consequently, n can be used to measure cooperativity and is thus an important parameter for analysis.

From the above considerations, simple analysis of the shift of apparent melting temperatures for protein complexes is insufficient to monitor an increase in macromolecular complex stability. We have illustrated this by two examples derived from raw experimental data (Supplementary Fig.4). In the first case, the unfolding transition represents an apparently two-state case (Supplementary Fig.4a). In this scenario both Boltzmann (used in DSF) and ProteoPlex data approximations schemes recapitulate the data with the exception that the latter based on the above described thermodynamic framework is capable of approximating the entire transition. In the second case, the unfolding transition is distinctly multiphasic and only the ProteoPlex approach is capable of approximating the experimental data, while the Boltzmann method fails (Supplementary Fig.4b). In conclusion, in the case of thermal unfolding of a macromolecular complex the apparent T_m is only a weighted average resulting from several superimposed unfolding curves that does not provide information about stability. However, information about cooperativity is proportional to apparent ΔH_m values and can hence be deduced by the slope of the transition. Thus, a shift of T_m to higher values is only meaningful when the slope of the transition increases or remains constant.

Data filtering and hierarchical sorting of conditions

A prerequisite to harness the power of ProteoPlex measurements is to rapidly identify stabilizing conditions and discard useless ones. To achieve this effectively, we have developed a data filtering and hierarchical sorting approach based on the over 80 examples we have measured thus far (Fig.5c and Supplementary Fig.1 and Supplementary Table 1). The present data filtering and hierarchical sorting scheme entails 6 steps: **1)** It starts with the identification of non-valid unfolding transitions. Those with more than 6 relevant local maxima, as well as buffer and water reference samples are removed from further calculation. **2)** The buffer references are averaged and the average is subtracted from all the unfolding transitions. **3)** The data is normalized by setting the lowest local minimum of each individual unfolding transition to 0 and the highest local maximum to 1000 (each identified by the first derivative of the transition). All absolute values below the lowest local minimum are discarded. **4)** Unfolding transitions from conditions containing air bubbles, which would falsify the

fluorescence signals representing the unfolding transitions, are removed. Since air bubbles induce high light scattering these conditions are readily identified by applying a specific threshold of the slope from the first data-point to the first local minimum. **5)** Fits are found for the remaining unfolding transitions based on the thermodynamic framework, defined and described above (equations (8) and (9)). Fits are run iteratively assuming cooperativity values n = 1-6. **6)** For these fits the ΔH_m, T_m and R^2 values are extracted and compared by R^2 analysis to an idealized two-state unfolding model.

Although this approach is quantitative, it should be noted that it provides only a qualitative guideline. T_m can be accurately determined to 0.5 K, but errors in ΔH_m can range up to 30%. This is due to the fact that the ΔH_m is strongly affected by small concentration errors. Additionally, a number of effects contribute to the ΔH_m value, of which complex disassembly, unfolding, and hydration enthalpies represent the largest proportion. Taken together, by employing a scheme with three steps of data preparation, filtering, and another three steps of hierarchical sorting and dynamical thresholding, stabilizing conditions for the sample under study can be found in an automated manner.

Although a complete cooperativity of unfolding seems very unlikely for large multi-subunit complexes, we and others have repeatedly found conditions exhibiting a near two-state unfolding behavior for all complexes tested so far. For all these, we obtained ΔH and T_m values in the expected order of magnitude of about 500 kJ/mol and 330 K, respectively. Notably, at the present state, we are unable to comment how these values for ΔH and T_m compare with experimentally determined values. We have been unable to find references in the literature for comparison. However, when considering that a buried surface area of 1 $Å^2$ in proteins is energetically equivalent to approximately 0.1 kJ/mol[4], our values would correspond to surface buried areas of 5000 $Å^2$. Such a value is well within the accumulated buried surface areas to be expected in multi-subunit macromolecular complexes.

Supplementary Table 1. Composition of custom made buffer screen. Column 12 is intentionally left blank for controls

	1	2	3	4	5	6	7	8	9	10	11	12
A	1 M SPG[1)] Buffer, pH 5.6	1M MMT[2)] Buffer, pH 5.6	1M PCB[3)] Buffer, pH 5.6	1M MES[4)] Buffer, pH 5.5	1M Na Citrate Buffer, pH 5.5	1M BisTris[5)] Buffer, pH 5.8	1M Na/K Phosphate Buffer, pH 5.8	1M ADA[6)] Buffer, pH 6.0	1M HEPES[7)] Buffer, pH 6.8	1M Imidazole Buffer, pH 6.2	1 M Tris[8)] Buffer, pH 7.5	
B	1 M SPG[1)] Buffer, pH 6.0	1M MMT[2)] Buffer, pH 6.0	1M PCB[3)] Buffer, pH 5.0	1M MES[4)] Buffer, pH 5.7	1M Na Citrate Buffer, pH 5.75	1M BisTris[5)] Buffer, pH 6.0	1M Na/K Phosphate Buffer, pH 6.1	1M ADA[6)] Buffer, pH 6.2	1M HEPES[7)] Buffer, pH 7.0	1M Imidazole Buffer, pH 6.45	1 M Tris[8)] Buffer, pH 7.7	
C	1 M SPG[1)] Buffer, pH 6.4	1M MMT[2)] Buffer, pH 6.4	1M PCB[3)] Buffer, pH 6.4	1M MES[4)] Buffer, pH 5.9	1M Na Citrate Buffer, pH 6.0	1M BisTris[5)] Buffer, pH 6.2	1M Na/K Phosphate Buffer, pH 6.4	1M ADA[6)] Buffer, pH 6.4	1M HEPES[7)] Buffer, pH 7.2	1M Imidazole Buffer, pH 6.7	1 M Tris[8)] Buffer, pH 7.9	
D	1 M SPG[1)] Buffer, pH 6.8	1M MMT[2)] Buffer, pH 6.8	1M PCB[3)] Buffer, pH 6.8	1M MES[4)] Buffer, pH 6.1	1M Na Citrate Buffer, pH 6.25	1M BisTris[5)] Buffer, pH 6.4	1M Na/K Phosphate Buffer, pH 6.7	1M ADA[6)] Buffer, pH 6.6	1M HEPES[7)] Buffer, pH 7.4	1M Imidazole Buffer, pH 6.95	1 M Tris[8)] Buffer, pH 8.1	
E	1 M SPG[1)] Buffer, pH 7.2	1M MMT[2)] Buffer, pH 7.2	1M PCB[3)] Buffer, pH 7.2	1M MES[4)] Buffer, pH 6.3	1M Na Citrate Buffer, pH 6.5	1M BisTris[5)] Buffer, pH 6.6	1M Na/K Phosphate Buffer, pH 7.0	1M ADA[6)] Buffer, pH 6.8	1M HEPES[7)] Buffer, pH 7.6	1M Imidazole Buffer, pH 7.2	1 M Tris[8)] Buffer, pH 8.3	
F	1 M SPG[1)] Buffer, pH 7.6	1M MMT[2)] Buffer, pH 7.6	1M PCB[3)] Buffer, pH 7.6	1M MES[4)] Buffer, pH 6.5	1M Na Citrate Buffer, pH 6.75	1M BisTris[5)] Buffer, pH 6.8	1M Na/K Phosphate Buffer, pH 7.3	1M ADA[6)] Buffer, pH 7.0	1M HEPES[7)] Buffer, pH 7.8	1M Imidazole Buffer, pH 7.45	1 M Tris[8)] Buffer, pH 8.5	
G	1 M SPG[1)] Buffer, pH 8.0	1M MMT[2)] Buffer, pH 8.0	1M PCB[3)] Buffer, pH 8.0	1M MES[4)] Buffer, pH 6.7	1M Na Citrate Buffer, pH 7.0	1M BisTris[5)] Buffer, pH 7.0	1M Na/K Phosphate Buffer, pH 7.6	1M ADA[6)] Buffer, pH 7.2	1M HEPES[7)] Buffer, pH 8.0	1M Imidazole Buffer, pH 7.7	1 M Tris[8)] Buffer, pH 8.8	
H	1 M SPG[1)] Buffer, pH 8.4	1M MMT[2)] Buffer, pH 8.4	1M PCB[3)] Buffer, pH 8.4	1M MES[4)] Buffer, pH 6.9	1M Na Citrate Buffer, pH 7.25	1M BisTris[5)] Buffer, pH 7.2	1M Na/K Phosphate Buffer, pH 7.9	1M ADA[6)] Buffer, pH 7.4	1M HEPES[7)] Buffer, pH 8.2	1M Imidazole Buffer, pH 7.95	1 M Tris[8)] Buffer, pH 9.0	

1) 1M SPG Buffer contains: 0.125 M Succinic Acid, 0.5 M NaH_2PO_4, 0.375 M Glycine adjusted to the appropriate pH with 10 M NaOH.
2) 1 M MMT Buffer contains: 0.2 M DL-Malic Acid, 0.4 M MES Monohydrate, 0.4 M Tris adjusted to the appropriate pH with either 10 M HCl or 10 M NaOH.
3) 1 M PCB Buffer contains: 0.4 M Sodium Propionate, 0.2 M Sodium Cacodylate trihydrate, 0.4 M Bis-Tris Propane adjusted to the appropriate pH with 10 M HCl.
4) MES (2-(N-morpholino)ethanesulfonic acid) monohydrate
5) Bis(2-hydroxyethyl)amino-tris(hydroxymethyl)methane
6) N-(2-Acetamido)iminodiacetic acid
7) 4-(2-Hydroxyethyl)piperazine-1-ethanesulfonic acid
8) 2-Amino-2-hydroxymethyl-propane-1,3-diol

Supplementary Table 2. Composition of custom made Additive screen. All conditions except G1 and F2 are adjusted to pH 7.0. Column 12 is intentionally left blank for controls

	1	2	3	4	5	6	7	8	9	10	11	12
A	1.5 M NaCl	0.5 M K_2SO_4	50% v/v	50 mM DTT [1]	50 mM Spermine	0.5 M L-Glutamic Acid	10 mM ATP [2]	50 mM Na Malonate	20 % v/v Methanol	0.1 M Guanidinium-chloride	0.1 M IPTG [3]	
B	1.5 M KCl	1 M KF	50% w/v Sucrose	50 mM TCEP [4]	50 mM Spermidine	0.5 M L-Aspartic Acid	10 mM ADP [5]	50 mM Na Pyruvate	20 % v/v Ethanol	0.1 M Urea	50 mM AICA [6]	
C	0.25 M $MgCl_2$	1 M KBr	50 % w/v Glucose	50 mM reduced Glutathion	50 mM Putrescine	0.5M L-Cysteine	10 mM AMPPCP [7]	50 mM L-Citrulline	20 % v/v Propanol	0.1 M NH_4SO_4	50 mM Polyvinyl Pyrrolidone	
D	0.25 M $CaCl_2$	1M KI	50% w/v Maltose	50 mM oxidized Glutathion	50 mM Taurine	1.5 mM L-Tyrosine	10 mM CMP [8], GMP [9], TMP [10], UMP [11]	50 mM Na Citrate	20 % v/v DMSO [12]	1 % w/v Protamine Sulfate	1 % w/v myo Inositol	
E	1.5 M LiCl	1 M KOAc	50% w/v Trehalose	50 mM EDTA [13]	50 mM Betaine	0.5 M L-Proline	10 mM NAD^+ [14]	50 mM Na Glutarate	2 % v/v Phenol	0.1 M Trimethylamine	1 % w/v tRNA [15]	
F	1.5 M NH_4Cl	1 M K_2S	50% w/v Galactose	50 mM Ascorbic Acid	0.5 M L-Arginine	0.5 M Glycine	10 mM NADH [16]	50 mM Na Succinate	2 % v/v Acetone	10 % w/v PEG [17] 6000	1 % w/v Glycogene	
G	0.25 M $ZnCl_2$	1 M KNO_3	10 % v/v PEG [17] 400	50 mM β-mercapto-ethanol	0.5 M L-Lysine	0.25 M L-Histidine	10 mM Biotin	1 mM Coenzyme A	20 % v/v DMF [18]	10 % w/v PEG [17] 10000	1 % DNA pieces [19]	
H	0.25 M $MnCl_2$	1M $KHPO_4$	10 % v/v Ethylene Glycol	50 mM MESNA [20]	0.15 M L-Asparagine	0.5 M L-Serine	10 mM Thiamine pyro-phosphate	Trace element mix [21]	20 % v/v Acetonitrile	0.05 % w/v OGP [22]	1 % w/v peptide mix [23]	

1) Dithiothreitol
2) Adenosinetriphosphate
3) Isopropyl β-D-1-thiogalactopyranoside
4) Tris(2-carboxyethyl)phosphine
5) Adenosinediphosphate
6) 5-Aminoimidazole-4-carboxamide
7) β,γ-Methyleneadenosine 5′-triphosphate
8) Cytidinemonophosphate
9) Guanosinemonophosphate
10) Thymidinemonophosphate
11) Uridinemonophosphate
12) Dimethylsulfoxide
13) Ethylenediaminetetraacetic acid
14) Nicotinamideadeninedinucleotide
15) Transfer ribonucleic acid
16) Nicotinamideadeninedinucleotide (reduced form)
17) Polyethyleneglycol
18) Dimethylformamide
19) low molecular weight DNA, from salmon sperm
20) 2-Mercaptoethanesulfonic acid sodium salt
21) 50 μM $FeCl_3$, 20 μM $CaCl_2$, 10 μM $MnCl_2$, 10 μM $ZnSO_4$, 2 μM $CoCl_2$, 2 μM $CuCl_2$, 2 μM $NiCl_2$, 2 μM Na_2MoO_4, 2 μM Na_2SeO_3, 2 μM H_3BO_3
22) Octyl β-D-glucopyranoside
23) NH2-RANDOM6AA-CONH2 (hydrophobic aa: F, A, L, M, I, W, P and V are excluded)

Supplementary Table 3. Overview of 84 complexes analyzed by ProteoPlex.
(a) Complexes come from all branches of life. (b) Besides multimeric complexes also single-chain proteins comprising multiple domains were analyzed. (c) Subcellular localization of the complexes measured. (d) All complexes analyzed show a broad range of different functions.

(a)

Organism group	Number of analysed complexes
Bacteria	10
Plantae	1
Fungi	23
Animalia	47
Archea	1
viral	2

(b)

Number of Chains	Number of analysed complexes
1 (multi-domain)	13
2 to 4	18
5 to 8	19
9 to 15	4
more than 15	30

(c)

Subcellular localisation	Number of analysed Complexes
Extracellular	7
Cytoplasmic	40
Mitochondrial	6
Nucleoplasmic	31

(d)

Function	Number of analysed complexes
Metabolic enzyme	4
Scaffolding protein	3
Chaperone	7

Nature Methods: doi:10.1038/nmeth.3493

mRNA-metabolism	25
Transcription	5
Translation	6
Proteostasis	6
Subcellular transport	20
molecular motor	4
Miscellaneous	4

Supplementary Table 4. Purification procedures / Sources for complexes utilized in the proof of principle experiments discussed in the present manuscript.

Complex	Purification procedure described in
Biomphalaria glabrata Hemoglobin	Lieb et al.[5]
Human (HeLa) 80S ribosomes	Khatter et al.[6]
Human Anaphase Promoting Complex	Frye et al.[7]
E.coli SelA	Forchhammer et al.[8]
E.coli GroEL/GroES	Bought from Sigma Aldrich
E.coli PDHc	Koike et al. [9]

Supplementary References

1. Niesen, F.H., Berglund, H. & Vedadi, M. The use of differential scanning fluorimetry to detect ligand interactions that promote protein stability. *Nature protocols* **2**, 2212-2221 (2007).
2. Clarke, J. & Fersht, A.R. Engineered disulfide bonds as probes of the folding pathway of barnase: increasing the stability of proteins against the rate of denaturation. *Biochemistry* **32**, 4322-4329 (1993).
3. Matouschek, A., Matthews, J.M., Johnson, C.M. & Fersht, A.R. Extrapolation to water of kinetic and equilibrium data for the unfolding of barnase in urea solutions. *Protein engineering* **7**, 1089-1095 (1994).
4. Raschke, T.M., Tsai, J. & Levitt, M. Quantification of the hydrophobic interaction by simulations of the aggregation of small hydrophobic solutes in water. *Proceedings of the National Academy of Sciences of the United States of America* **98**, 5965-5969 (2001).
5. Lieb, B. et al. Red blood with blue-blood ancestry: Intriguing structure of a snail hemoglobin. *Proceedings of the National Academy of Sciences* **103**, 12011-12016 (2006).
6. Khatter, H. et al. Purification, characterization and crystallization of the human 80S ribosome. *Nucleic acids research* **42**, e49 (2014).
7. Frye, J.J. et al. Electron microscopy structure of human APC/C(CDH1)-EMI1 reveals multimodal mechanism of E3 ligase shutdown. *Nature structural & molecular biology* **20**, 827-835 (2013).
8. Forchhammer, K., Leinfelder, W., Boesmiller, K., Veprek, B. & Bock, A. Selenocysteine synthase from Escherichia coli. Nucleotide sequence of the gene (selA) and purification of the protein. *The Journal of biological chemistry* **266**, 6318-6323 (1991).
9. Koike, M., Reed, L.J. & Carroll, W.R. alpha-Keto acid dehydrogenation complexes. IV. Resolution and reconstitution of the Escherichia coli pyruvate dehydrogenation complex. *The Journal of biological chemistry* **238**, 30-39 (1963).
10. Barrick, D. Replacement of the proximal ligand of sperm whale myoglobin with free imidazole in the mutant His-93-->Gly. *Biochemistry* **33**, 6546-6554 (1994).